JOURNAL OF MATERIALS SCIENCE 29 (1994) 3200–3208

Ceramic joining II
Partial transient liquid-phase bonding of alumina via Cu/Ni/Cu multilayer interlayers

M. L. SHALZ, B. J. DALGLEISH, A. P. TOMSIA, A. M. GLAESER
Center for Advanced Materials, Lawrence Berkeley Laboratory, and Department of Materials Science and Mineral Engineering, University of California, Berkeley, California 94720, USA

Multilayer Cu/Ni/Cu interlayers that form a thin layer of a Cu-rich transient liquid phase have been used to join alumina to alumina at 1150 °C. The method and bonding conditions yield an assembly bonded by a Ni-rich (>94 at% Ni) interlayer at a temperature substantially lower than those normally required for solid-state diffusion bonding with pure Ni interlayers. Flexure strengths of as-bonded beams ranged from 61 to 267 MPa with an average of 160 MPa and a standard deviation of ±63 MPa. The highest flexure strengths were observed in samples where failure occurred in the ceramic. Post-bonding anneals of 10 h duration in air and gettered-argon at 1000 °C decreased the average room temperature strength to 138 and 74 MPa, respectively. In as-processed and annealed samples, varying degrees of interfacial spinel formation are indicated. Spinel formation may contribute to the scatter in as-processed samples, and the decrease in strength values resulting from annealing.

1. Introduction

Both solid-state diffusion bonding [1, 2] and reactive metal brazing [2, 3] have been explored extensively as methods of producing strong joints for high-stress, high-temperature applications. In principle, both methods have the potential to produce strong joints. In practice, the difficulties associated with fabricating reliable joints using these methods increase with projected use temperature and stress levels. In general, as the intended operating temperature increases, and more refractory metal interlayers or brazing alloys are used, bonding temperatures or bonding pressures (or both) increase, and the tendency for interfacial reactions and the potential for degrading the microstructure and properties of the materials to be joined also increases. The severe difficulties that arise when diffusion bonding and brazing are applied to forming joints for high temperature use is at least in part a consequence of the more demanding processing conditions imposed by the use of chemically homogeneous interlayers.

Recent work by Iino [4, 5] and by Glaeser *et al.* [6–9] has explored the use of inhomogeneous interlayers for joining. These microdesigned multilayer interlayer structures form a transient liquid phase at relatively low temperatures to facilitate joining with refractory metal-based interlayers. A thin film of a lower melting point metal (e.g. Cu) or alloy that melts during bonding is deposited onto a much thicker foil of a more refractory metal (e.g. Ni, Pt, Nb) or alloy (e.g. 80Ni20Cr) as illustrated in Fig. 1a,b. The two metals or alloys are selected such that the more refractory metal incorporates the less refractory component by interdiffusion (or consumes it by reaction) at the bonding temperature, and produces a suitably refractory alloy (or reaction product). Ideally, such a method melds the best features of solid-state and liquid-based joining methods. As a result, interlayer and assembly properties and performance capabilities that are difficult or impractical to achieve using conventional joining methods become more accessible.

The simplest interlayer design uses components that form complete solid solutions. In the absence of reactions with the ceramic, the equilibrium state for the interlayer is a solid solution with an overall composition reflecting the interlayer design, as illustrated schematically in Fig. 1c. In previous work [6], Cu/Pt/Cu interlayers, which form a Pt-rich solid solution at elevated temperature, were used to successfully join alumina. The significant difference between the melting temperatures of Cu (1085 °C) and of Pt (1769 °C) allowed a substantial decrease in the processing temperature relative to those reported for diffusion bonding [10–13] or required for brazing with pure Pt [11].

This paper represents an extension of the experimental methods in [6], and reports the results of preliminary experiments exploring the joining of Al_2O_3 ceramics via multilayer Cu/Ni/Cu interlayers. The Cu–Ni system also exhibits complete mutual solid solution at elevated temperature, and there is a significant difference between the melting point of Cu (1085 °C) and Ni (1453 °C). Thus, as for Cu/Pt/Cu interlayers, the possibility of reducing the processing temperature relative to those normally used for brazing and diffusion bonding was anticipated.

0022–2461

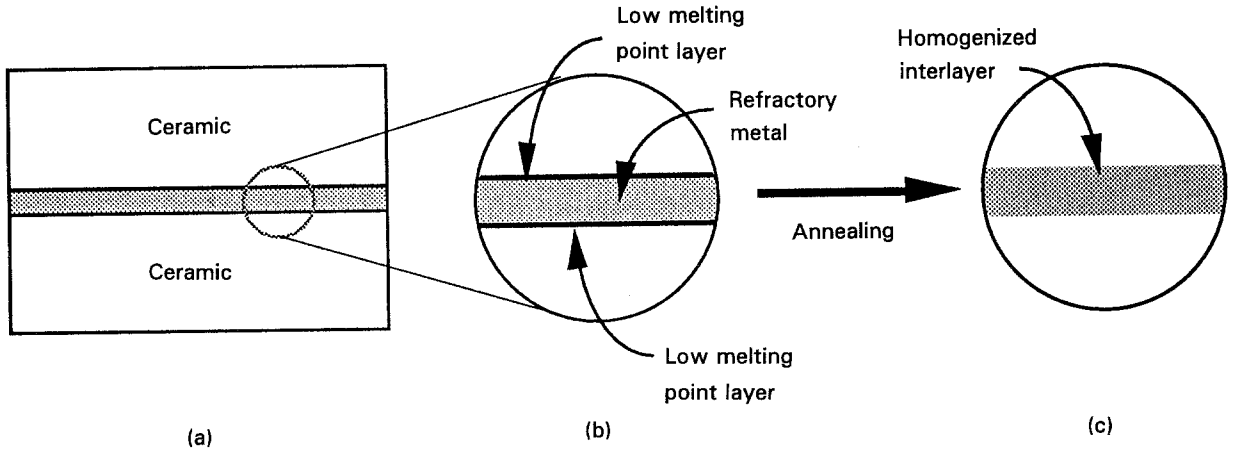

Figure 1 Schematic illustration of (a) ceramic/interlayer/ceramic assembly, (b) detail of microdesigned interlayer prior to heating, and (c) uniform interlayer after partial transient liquid phase bonding or solid-state bonding (and possibly additional heat treatment).

2. Background

A detailed discussion of joining and the use of multilayer interlayers that form a thin or partial layer of a transient liquid, so-called partial transient liquid phase (PTLP) bonding, has been provided in [6, 7]. The focus of this discussion is prior work on the wetting behaviour of Ni on alumina that is relevant to brazing, and studies of diffusion bonding of $Al_2O_3/Ni/Al_2O_3$ assemblies with particular attention to the issue of spinel formation.

Several studies have examined the wetting characteristics of Ni on alumina substrates [e.g. 14–17]. Although there are differences in the purity of the Ni used, the specific form and purity of alumina used, and the temperature range examined, one general conclusion emerges from the studies – pure Ni droplets generally form obtuse contact angles on alumina. Reactive metal additions are necessary to decrease the contact angle and provide wetting behaviour more amenable to joining via brazing. Studies of the wetting characteristics of Ni-rich Ni–Ti [15, 16] and Ni–Cr alloys [15, 17] on Al_2O_3 have shown that Ti and Cr additions reduce the contact angle of molten Ni-rich droplets on alumina. At sufficiently high Ti and Cr levels, contact angles of $\leqslant 90°$ are obtained at 1500 °C, however the high processing temperatures have in part encouraged exploration of solid-state joining routes.

There have been several studies of diffusion bonding of Al_2O_3 to Ni [12, 13, 18–20]. A summary of bonding conditions is provided in Table I. When bonding stresses are too low, as in the work of Gee [18], weak bonds are formed even at elevated temperature. The results of Klomp [12] show a trend towards higher strength with increasing bonding stress. The results of Calow & Porter [19] show that weak bonds result if the bonding temperatures (e.g. 700 °C) are too low. Generally the bonding temperatures required to form strong diffusion bonds are a significant fraction of the melting point of Ni, consistent with trends observed in other ceramic/metal systems [3, 10, 11]. Numerous factors, including the formation of interfacial reaction layers, can contribute to the development of a maximum bond strength at some intermediate temperature.

The bonding temperature, Ni purity and atmosphere can play an important and interactive role in determining the microchemical and microstructural evolution of the Ni/Al_2O_3 interface [20, 21]. Wasynzuk & Rühle [20] performed a TEM investigation of Ni/Al_2O_3 diffusion bonds prepared at 1390 °C (see Table I) under high vacuum conditions (10^{-8} atm). A reaction layer ≈ 1 μm thick of nickel aluminate spinel, nominally $NiAl_2O_4$, was found. When a specimen diffusion bonded under high vacuum conditions was subsequently annealed for 2 h at 1390 °C under very high vacuum conditions (10^{-10} atm), the spinel layer disappeared [21]. Diffusion bonding experiments conducted under high vacuum conditions utilizing oxygen-free and oxygen-containing Ni foils have demonstrated the existence of a threshold oxygen activity for spinel formation at the interface [21], and that the source of the oxygen necessary to drive spinel formation can be the oxygen dissolved in the Ni. The

TABLE I Ni/Al_2O_3 diffusion bonding conditions

Reference	Pressure (MPa)	Bonding time (min)	Temperature (°C)	Strength (MPa)
Klomp [12]	1.5, 9.8, 98	20	1350	47, 64, 196
Gee [18]	2.2×10^{-3}	180	1300	All samples failed during handling
		180	1400	
Calow & Porter [19]	31	120	700–1300	$\leqslant 70$ with peak strength at 950 °C suggested
Wasynczuk & Rühle [20]	4	120	1390	Not evaluated
Trumble & Rühle [21]	4	120	1390	Not evaluated

threshold dissolved oxygen content for spinel formation increases with temperature, and is given by the expression

$$[\text{at \%O}_{\text{Ni(s)}}] = \exp\left(\frac{-7550 \pm 1200}{T} + 0.84\right)$$

which assumes values of ≈ 60 at p.p.m. and 115 at p.p.m. at 1000 and 1150 °C, respectively [21].

3. Experimental procedure

The experimental procedures used in this study are virtually identical to those employed in the bonding of alumina using multilayer Cu/Pt/Cu interlayers, and reported previously [6]. As a result, only a brief description of the procedures is given here.

3.1. Materials

The polycrystalline alumina (Coors, Golden, Colorado, USA) used was $\approx 98\%$ dense and 99.5% pure, and contained a small amount of silicate phases. The material was in the form of $19.5 \times 20.0 \times 22.5$ mm^3 blocks. The blocks were polished with successively finer grits of diamond in an oil slurry; the final polish was performed using 6-μm diamond paste. Following polishing, samples were cleaned in isopropyl alcohol, dried, and then air-annealed for 14 h at 1000 °C to remove organic surface contaminants.

The Ni foil (Puratronic grade foil; Johnson-Matthey Materials Technology, Herts, UK) was ≈ 100 μm thick, and reportedly 99.994 + wt % pure with respect to metallic impurities. In view of the possibility of spinel formation, an oxygen analysis on the foil was performed using an inert gas fusion method [22]. Results indicated levels were below the detection limit of the technique employed, nominally 10 wt p.p.m. (≈ 37 at p.p.m.) dissolved oxygen. The foil was cleaned in isopropyl alcohol, rinsed in nanopure distilled water (resistivity 18.3 MΩ cm), and dried with a heat gun prior to use.

The starting material for the copper deposition was a 99.8% pure commercial copper wire of unknown oxygen content. To prepare small copper sources for deposition, cleaned pieces of wire were melted in tungsten baskets under a vacuum ranging from $2\text{–}9 \times 10^{-6}$ torr.

3.2. Copper coating

Thin layers of copper were deposited directly onto the polished and cleaned alumina blocks in an evaporator. After introducing the alumina blocks, the chamber pressure was reduced to $\approx 3 \times 10^{-6}$ torr, and fluctuated between 7 and 10×10^{-6} torr during deposition. Weight gain and profilometry based methods were used to establish the thickness of the Cu layer. Both measurements indicate an average copper thickness of $\approx 3 \pm 0.3$ μm. The resulting Cu/Ni thickness ratio leads to an overall or average interlayer composition of ≈ 94.7 at % Ni.

3.3. PTLP bonding

The block/foil/block assembly was prepared immediately after coating, and bonding of the assembly was performed in a graphite die in a vacuum hot press. The temperature was raised to 1150 °C at 4 °C min^{-1}, maintained at 1150 °C for 6 h, and then lowered to room temperature at 2 °C min^{-1}. During this cycle, the vacuum in the press was in the range of 8×10^{-6} to 2×10^{-5} torr, and a pressure of ≈ 5.1 MPa was maintained on the assembly.

3.4. Beam preparation

Five plates were cut from the bonded block assembly using a diamond wafering saw. Subsequently, one surface of each plate was polished on a vibratory polisher using progressively finer grit size (30, 15, 6 μm) diamond paste in an oil slurry. Beams of approximately square cross-section ($\approx 3.4 \times 3.4$ mm) were cut from the polished plates with the metal interlayer at the beam centre. The tensile edges of flexure beams were bevelled to remove machining flaws that could initiate failure.

3.5. Post-bonding heat treatments

Beams from plates 3 and 4 were annealed for 10 h at 1000 °C. Plate 3 was annealed in air, while plate 4 was annealed in flowing > 99.998% purity argon (oxygen-gettered with a mixture of titanium and zirconium chips). The principal objective of these anneals was to determine whether environmental exposure affected the flexure strength.

3.6. Flexure testing

Beams were tested at room temperature using four-point bending with an inner span of 8 mm, outer span of 25 mm and a displacement rate of 0.05 mm min^{-1}. Strengths were calculated from the load at failure using standard relationships derived for monolithic elastic materials.

3.7. Microstructural and microchemical characterization

One polished as-bonded bend beam was examined prior to mechanical testing using energy dispersive spectroscopy (EDS) to evaluate the extent of diffusion of copper into nickel during the complete bonding cycle. Line scans were conducted perpendicular to the interface. The electron beam diameter is typically of the order of 1 μm, and a typical detection limit is ≈ 1 at %, and thus we anticipated that this method would provide information on the extent of homogenization achieved during the bonding cycle.

After mechanical testing, beam fracture surfaces were mounted adjacent to one another so that equivalent fractographic locations were in mirror symmetry positions. The general appearance of the microstructure at matching locations could thus be readily identified. Fracture surfaces were inspected visually using optical microscopy, and finally examined using scanning electron microscopy (SEM) and EDS.

The ceramic surfaces of some fractured specimens exhibited a blue discoloration, attributed to spinel formation. Thin-film X-ray diffraction analysis was carried out. A monochromatic beam of CuK_α was focused at an incidence angle of 1°. The sample surface is held stationary with respect to the incident X-ray while the special detector holder with soller slits is rotated to the appropriate 2θ angles. This method increases the effective volume of diffraction and enhances the diffraction signal from samples with a small amount of a second phase present as a thin film on the surface.

4. Results and discussion

4.1. Microchemical characterization

Results of the EDS line scan taken perpendicular to the Al_2O_3/Ni foil interface are shown in Fig. 2. The Cu concentration is essentially constant across the interlayer; the values range from 5.1 to 6.2 at %. The average Cu concentration for the entire interlayer, $\approx$ 5.6 at %, lies within these bounds, and is in reasonably good agreement with the overall interlayer composition (5.3 at % Cu) calculated from the relative Cu and Ni thicknesses. The Cu concentration does not decrease smoothly from the edge to the centre of the interlayer. The slight variations in composition that are evident do not appear to reflect a residual compositional gradient that would decay with further annealing, but instead appears to reflect instrumental variability. When analyses from areas whose centres were within 1 μm of one another were compared, Cu concentrations from adjacent sampling areas differed by up to $\pm$ 0.5 at %. There is every indication that the interlayer has completely homogenized during the bonding cycle. The solidus temperature for a Cu–Ni alloy containing 6.2 at % Cu is of the order of 1430 °C [23], and thus approaches the melting temperature of pure Ni. From a practical perspective, the results indicate that it may be possible to reduce the bonding time without substantially affecting the homogeneity of the interlayer.

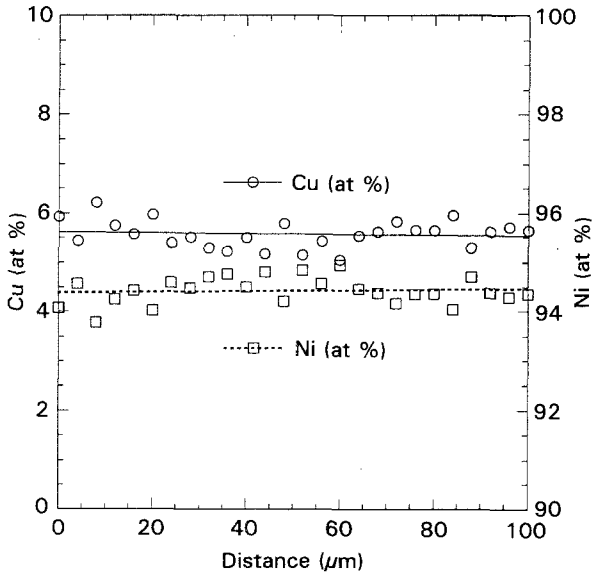

Figure 2 Chemical profiles of Cu and Ni in the interlayer of an as-bonded sample as determined by EDS. Note the difference in the scales for Cu and Ni. Complete homogenization of the interlayer is indicated; the minimum solidus temperature in the interlayer is of the order of 1430 °C, and well above the initial bonding temperature. (For clarity, not all data points are shown.)

4.2. Fracture of as-bonded beams

The results of flexure tests of as-bonded beams are included in Table II, and plotted in Fig. 3. Failure strengths of as-processed beams ranged from $\approx$ 61 to 267 MPa with an average value of 160 MPa. For comparison, the average four-point bend strength of (unbonded) alumina beams prepared from the same source and tested under the same test conditions is $\approx$ 280 MPa. The overall scatter in the failure strengths of as-processed beams is larger than observed in Cu/Pt/Cu [6] and Cu/Nb/Cu [9] bonded assemblies.

The strongest as-processed beams (259 and 267 MPa) had strengths approaching the average strength of the (unbonded) ceramic, similar to the behaviour observed previously in Cu/Pt/Cu bonded assemblies. Failure in these samples originated in and propagated through the ceramic. The results demonstrate the potential for forming strong joints.

Three of the twelve as-bonded samples tested failed along one of the two ceramic/metal interfaces. In these samples, comparisons of the corresponding regions of the ceramic and metal sides of the fracture surface indicate that intimate ceramic–metal contact was achieved, as demonstrated by the imprint of the ceramic microstructure on the metal foil. However, there are also regions in which contact is not complete, reminiscent of observations in the lower-strength Cu/Pt/Cu bonded assemblies [6]. Fig. 4 shows examples of featureless regions that appear on the metal side of the fracture surface. These must be depressions in the interlayer, possibly caused by a local failure of the liquid film to wet the ceramic substrate. When the corresponding region on the ceramic fracture surface is examined, there is a strong correlation between the location of these regions and pores or larger voids in the ceramic. Although these non-bonded regions are not large individually, they can occur with relatively great frequency and can locally occupy a sufficient fraction of the total interfacial area. In Fig. 4, which is from a sample with a failure strength of 136 MPa, the non-bonded regions account for nearly 20% of the interfacial region shown. In other areas of similar defect density, the individual defects are in close proximity to one another. When concentrated in this manner, these defects may have the combined effect of a large flaw and contribute to both the low failure strengths and the scatter.

There are also indications that spinel formation at the Ni/Al_2O_3 interface may have had an effect on the failure behaviour. In seven of twelve as-bonded samples, partial debonding occurred along the second ceramic/metal interface during fracture. In the weakest sample, the debonded region accounts for

TABLE II Flexure strengths (MPa)

Heat treatment	Plate	Beam 1	Beam 2	Beam 3	Beam 4	Mean for plate	Standard deviation
As-bonded	1	61	136	138	182		
		i,d	i	i	i,d	129	± 50
As-bonded	2	259	138	126	267		
		c	i,d,b	i,d,b	c	198	± 76
Air-annealed	3	172	163	97	122		
10 h @ 1000 °C		i,b	i,d,b	i,b	i,b	138	± 35
Argon-annealed	4	95	0	98	103		
10 h @ 1000 °C		i,b	i,h,b	i,b	i,d,b	74	± 49
As-bonded	5	177	218	119	95		
		i,d	i,b	i,d,b	i,d,b	152	± 56

Abbreviations: c = ceramic failure, i = interfacial failure, d = debonding on second ceramic/metal interface, b = bluish tint, h = broke during handling.

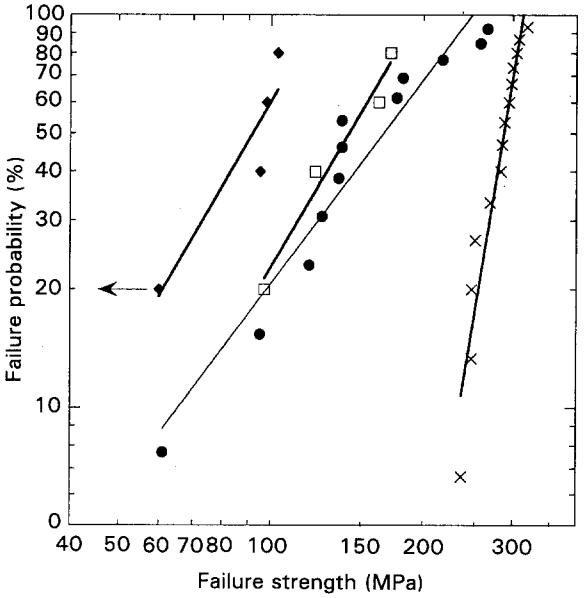

Figure 3 Plot of failure strength and failure probability for (●) as-bonded beams, (□) air-annealed, (◆) argon-annealed beams, and (×) data for unbonded alumina beams prepared from the same source material. For the argon-annealed samples, one of four beams failed during handling, and the strength of 60 MPa is intended as an upper estimate of the stresses applied during handling.

≈ 50% of the total ceramic/metal interface, as shown in Fig. 5. The debonding along the second ceramic/metal interface, and the formation of isolated pockets in which there is loss of contact, suggests regions of relatively weaker bonding. In five of the ten as-processed beams in which fracture exposed one or more ceramic surfaces, patches exhibiting a faint bluish hue were observed on the ceramic fracture surface. This coloration is attributed to the formation of $NiO–Al_2O_3$ spinel, nominally $NiAl_2O_4$. The interface between Ni and $NiAl_2O_4$ is suggested to be weak [21], and thus spinel formation could also introduce local relatively weaker regions along the ceramic–metal interface that degrade the strength and introduce scatter.

The observations suggesting spinel formation were somewhat surprising. The chemical analysis of the Ni foil indicated an oxygen level (⩽ 37 at p.p.m.) well below that required for spinel formation at 1150 °C (115 at p.p.m.). Post-bonding anneals in both an oxidizing atmosphere and a low oxygen partial pressure atmosphere were used to assess the tendency for spinel formation at a lower temperature with a lower threshold oxygen level (61 at p.p.m.), and to indicate the oxygen source for spinel formation.

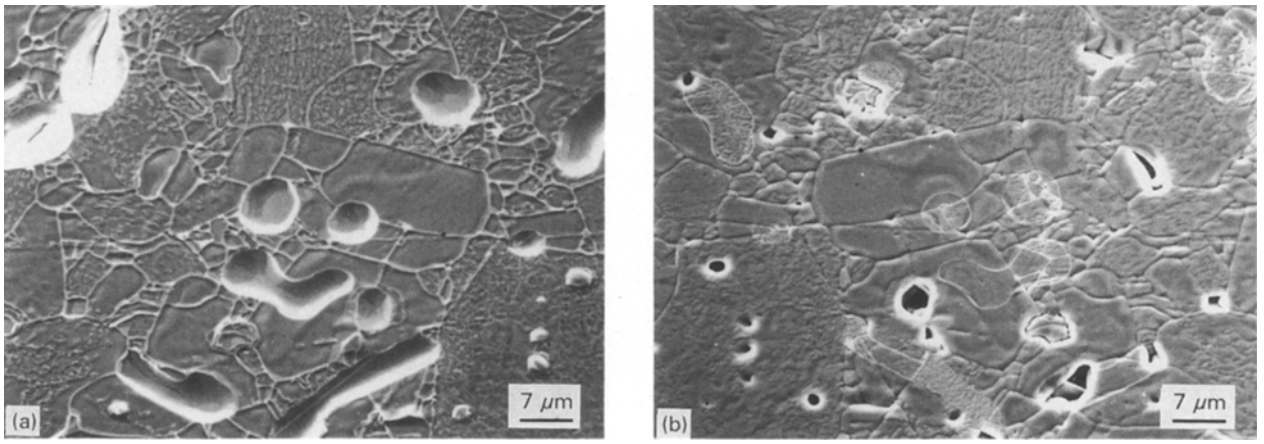

Figure 4 SEM micrographs of corresponding regions on the (a) metal and (b) ceramic sides of a fracture surface of an as-processed beam. The grain structure of the ceramic is imprinted on the metal foil where good contact was achieved. Local regions of poor contact that appear as featureless on the metal are also apparent. There appears to be a correlation between regions of poor contact and the location of pores or other microstructural defects in the ceramic.

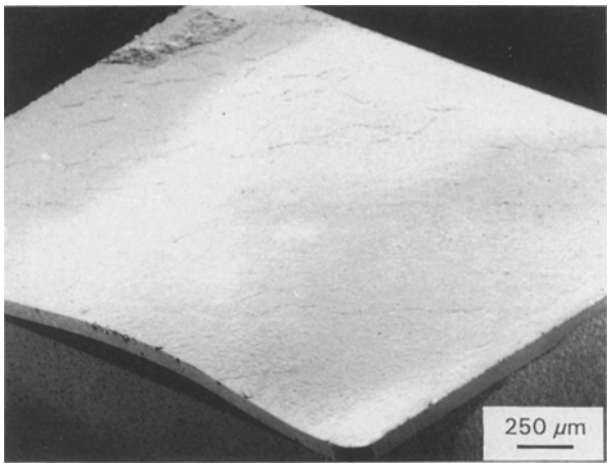

Figure 5 SEM micrograph of half of a failed beam in which debonding of the metal foil is particularly evident. The region in the upper left hand quadrant of the metal foil shows a small patch of adhering alumina grains. This beam exhibited a particularly low failure strength (61 MPa). Although the fracture path followed one ceramic/metal interface, partial debonding occurred along the second ceramic/metal interface of many samples.

4.3. Effects of post-bonding annealing at 1000 °C

Air annealing had two primary effects. Firstly, it appeared to reduce the average strength relative to that of as-processed samples (Fig. 3, Table I). Secondly, it caused the bluish hue to become more intense and evident over a larger fraction of the ceramic fracture surface, suggesting the formation of additional spinel during the anneal. At 1000 °C, the critical oxygen partial pressure for formation of spinel at pure Ni/Al_2O_3 interfaces is estimated to be 8.4×10^{-13} atm [21]. Although the critical oxygen partial pressure for a Ni-rich Cu–Ni alloy would be somewhat higher, air anneals at 1000 °C would be expected to promote the formation of a spinel layer. However, inward oxygen diffusion in pure Ni (and by assumption in Ni-rich Cu–Ni alloys) is expected to affect only a relatively thin band around the perimeter of the plate; $Dt^{1/2}$ is ≈ 180 μm for oxygen diffusion in pure Ni after 10 h at 1000 °C [24]. Although a (weakly bonded or defective) spinel layer extending ≈ 180 μm inward along the tensile edge could degrade the bend strength, more pervasive spinel formation at 1000 °C is suggested by the change in the intensity and spatial distribution of the spinel.

Although only a limited number of data are available, post-bonding argon annealing appears to decrease the strength relative to both as-processed and air-annealed samples (Fig. 3, Table I). The effect is not quite as pronounced as in Ar-annealed Cu/Pt/Cu bonded assemblies where all samples failed during handling [6]. A bluish hue was again evident on the ceramic fracture surface of all argon-annealed samples, despite an ambient oxygen partial pressure estimated to be $\approx 10^{-33}$ atm. This confirms that the oxygen source for spinel formation was the interlayer, i.e. that the dissolved oxygen content in the interlayer was above the threshold level necessary to stabilize the spinel phase at 1000 °C, and indicates that spinel formation competes successfully with outward diffusion of oxygen to decrease the oxygen content of the interlayer. In comparison to air anneals, the spinel may be degraded or decomposed along sample edges, and this may introduce relatively more severe flaws (e.g. physical gaps) along the tensile edges of beams.

4.4. Microchemical and microstructural analysis of reaction layer

Two samples subjected to post-bonding annealing were selected for further analysis designed to confirm that the discoloration was due to spinel, and to identify the effect of spinel formation on the fracture surface characteristics.

In one of the argon-annealed specimens, a sharp boundary between the white alumina and the blue region was evident on the fracture surface. Gold coating of the specimen accentuated the difference in the topography of the two regions of the fracture surface. In Fig. 6a, a low magnification SEM micrograph of the fracture surface is shown. There is a slight change in contrast between the (darker) unreacted region on the left, and the (lighter) blue region on the right. Fig. 6b shows the topography of the unreacted white region at higher magnification. There is a 'glazed' appearance to the majority of the fracture surface, reminiscent of the appearance of fracture surfaces in diffusion bonded $Al_2O_3/Pt/Al_2O_3$ assemblies [25]. In both cases, the results suggest that an amorphous silicate layer forms between the metal foil and the alumina during bonding. The ceramic microstructure is more sharply defined in the vicinity of defects (residual pores) in the ceramic, and the 'edges' of the glazed layer become evident. Thus it appears to be energetically favourable to replace the metal/alumina interface with a glass/alumina and a glass/metal interface where direct contact is achieved. Where direct contact is precluded by pores and surface cavities, the glassy phase is apparently not drawn to the surface. Dalgleish (unpublished data) has conducted Pt/Al_2O_3 diffusion bonding experiments in which depressions were introduced into the Pt foil prior to bonding using a hardness indentor. Examination of fracture surfaces showed that in the vicinity of the indents, where ceramic/metal contact was not achieved, the glassy phase was not drawn to the surface. In the present case, the regions that are glass-free extend well beyond the void perimeter. The cause of this behaviour is not known.

Thus, there are indications that the glassy phase may play a role in bond formation. Fig. 6c shows the topography of the blue region at higher magnification. The development of a faceted reaction product is suggested. EDS analysis of the faceted regions results in strong peaks attributable to Al, Ni, and O, and a very weak peak that may be due to Si. Similar EDS analysis of selected areas within the unreacted region shown in Fig. 6b, results in strong Al and O peaks, a very weak peak possibly due to Si, but no Ni peak. If the weak peaks do correspond to Si, this would be consistent with the observation of what appears to be

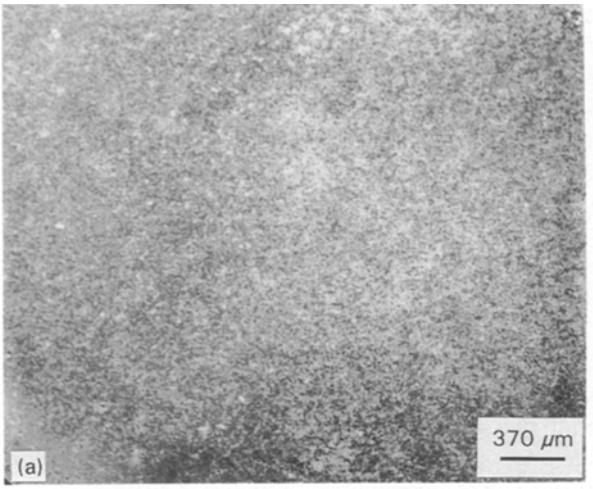

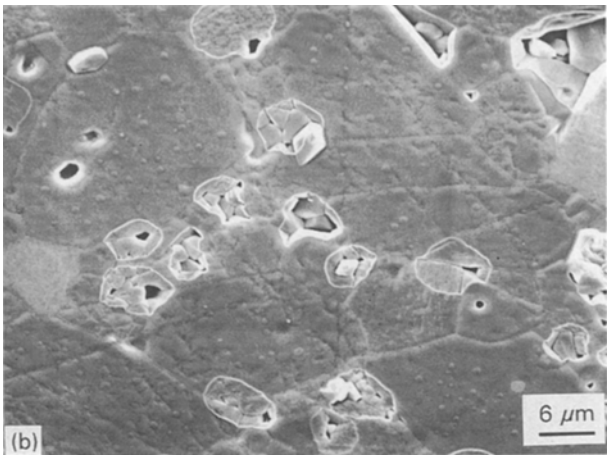

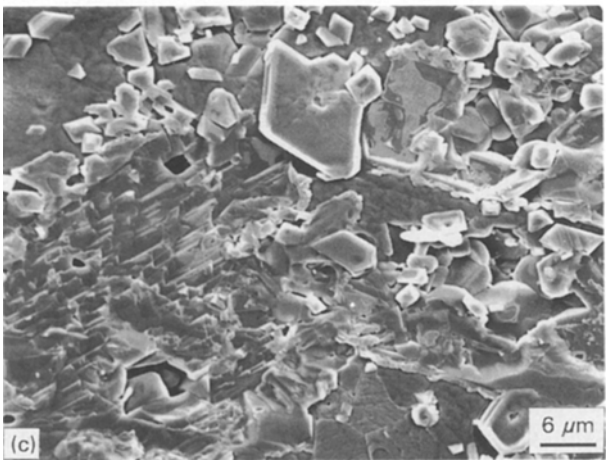

Figure 6 (a) Low magnification SEM micrograph of a ceramic fracture surface in an argon annealed sample in which a clear discontinuity in colour was evident. White, apparently unreacted region to the left; blue region on the right. There is a light difference in contrast. At higher magnifications, the topography, differences between (b) unreacted and (c) reacted regions are evident. In (b) the ceramic appears to be covered with a glassy film that is disrupted in the vicinity of surface pores. In (c) a faceted reaction product shown to contain Al, Ni and O is found.

a thin amorphous layer. In the unreacted region, failure appears to have occurred along the metal/silicate interface.

XRD analysis of the near-surface region of an annealed specimen produced a superposition of diffraction peaks attributable to Al_2O_3 and $NiAl_2O_4$ as shown in Fig. 7. For the diffraction conditions used, we estimate that the penetration depth of the X-ray beam was less than 0.5 μm. Qualitatively, the relative intensities of alumina and spinel peaks suggest that the spinel layer is the minor constituent of this $\leqslant 0.5$ μm thick surface layer, and thus, the spinel layer in even annealed specimens is < 0.2 μm thick. The spinel film thickness is determined by the difference between the initial oxygen content, the threshold oxygen content for spinel formation, and the foil thickness. Using the solubility limit of oxygen for Ni–NiO equilibrium at 1000 °C (≈ 460 p.p.m.) as an upper bound on the initial oxygen content, and 61 p.p.m. as the threshold value, a maximum possible spinel layer thickness of ≈ 0.15 μm is deduced.

The microstructural observations, EDS analysis and XRD results collectively establish that spinel is formed. At higher temperatures, where the threshold oxygen level is higher, less spinel is formed; the spinel apparent on some as-processed beams may have formed during slow cooling. At lower temperatures, where the threshold level is lower, spinel formation becomes more pronounced. Qualitatively, the trends are consistent with expectations derived from the results and analysis of Ni/Al_2O_3 diffusion bonding [21].

Quantitatively, there appear to be some disparities between predicted threshold levels and the results of chemical analysis. For a dissolved oxygen content of $\leqslant 37$ p.p.m., no spinel formation is expected under the experimental conditions used. Thus some assessment of possible sources of error in the predictions and the chemical analysis is warranted.

There are uncertainties in the thermodynamic data used to develop Equation 1. Taking the indicated uncertainty (± 1200) into account, we obtained upper

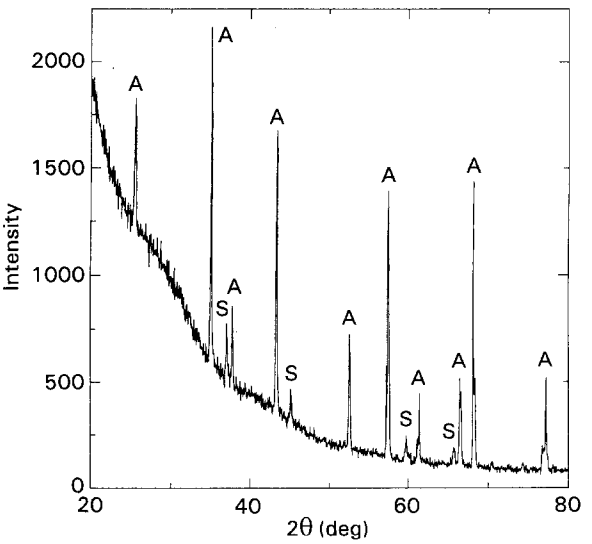

Figure 7 Diffraction pattern obtained from surface layer for 2θ values ranging from 20 to 80°. The peaks match those of Al_2O_3 (A) and $NiAl_2O_4$ spinel (S).

and lower limits for the threshold oxygen concentration of 270 and 50 at p.p.m. at 1150 °C. At 1000 °C, the corresponding upper and lower limits are 158 and 24 at p.p.m. The 50 at p.p.m. and 24 at p.p.m. values bound the detection limit for oxygen. Using the lower limits, one could account for spinel formation during cooling from the bonding temperature and more extensive spinel formation after annealing at 1000 °C. However, for oxygen levels between 24 and 50 at p.p.m., the spinel layer formed even after extensive annealing at 1000 °C would be extremely thin ($\approx$5 nm), and difficult to detect by even thin-film X-ray methods. Thus although the uncertainties in the threshold oxygen levels should not be neglected, it seems more likely that the oxygen content of the interlayer exceeds the level suggested by chemical analysis. In this regard, we note that the oxygen analysis was performed on the Ni alone, and does not include any oxygen that might have been incorporated in the Cu. As the copper films account for $\approx$5–6 at % of the total interlayer, the incorporation of just a few hundred p.p.m. oxygen in the copper layer would significantly affect the total interlayer oxygen content. The copper used may contain significant amounts of oxygen; no analysis was performed on the starting material because subsequent processing was expected to change the purity. The Sievert's Law coefficient for oxygen in copper is high at temperatures near and above the melting point of copper [26]. As a result, even though the ambient oxygen pressures during premelting and deposition are expected to be low, it is conceivable that the oxygen content within the deposited copper films is of the order of a few hundred p.p.m., and thus, sufficiently high to increase the oxygen content of the complete Cu–Ni interlayer above the threshold level for spinel formation.

5. Conclusions

The above results demonstrate the potential for forming strong bonds between Al_2O_3 and Ni-rich interlayers at relatively low temperatures using Cu-based transient liquids. The bonding conditions used completely homogenized the interlayer.

Beams that exhibited high strength and failed in the ceramic were produced. However, there was considerable scatter in the fracture strength. Local regions of poor contact between the ceramic and metal were evident. The underlying cause of these bonding defects is not known with certainty; however there is an indication that regions of poor contact preferentially arise in regions where defects exist in the substrate surfaces. Precoating substrates with Cr might improve the strength distribution by improving the wetting of the liquid film, and experiments assessing this possibility are in progress. Spinel formation was evident in as-bonded samples but more pronounced on the fracture surface of samples subjected to post-bonding anneals at 1000 °C. The annealed samples exhibited lower fracture strengths than as-bonded samples, suggesting that spinel formation may contribute to the scatter in as-processed samples, and the decrease in strength values resulting from annealing. The use of Ni foils with low(er) dissolved oxygen contents, coupled with processing modifications that reduce the oxygen content of the coating, may permit the fabrication of more uniformly strong bonds. A more extensive assessment of the roles of oxygen and glassy phases in the partial transient liquid phase bonding of Al_2O_3 via Cu/Ni/Cu interlayers is in progress.

Acknowledgements

This research was initiated while A. M. G. was on appointment as a Miller Research Professor in the Miller Institute for Basic Research in Science. Helpful discussions and correspondence with R. M. Cannon, Y. Iino, M. Nicholas, and J. A. Pask are acknowledged. The assistance of M. Locatelli and K. Nakashima is greatly appreciated. Special thanks are due to the Alcoa Foundation for providing the financial resources that allowed the first demonstration of this joining concept. Additional unrestricted grants from and equipment donations by ARCO, IBM, and DuPont contributed to the development of facilities used in this research. This work was supported by the Director's Exploratory Research and Development Fund of LBL under Contract No. DE-AC03-76SF00098.

References

1. K. SUGANUMA, Y. MIYAMOTO and M. KOIZUMI, *Ann. Rev. Mater. Sci.* **18** (1988) 47.
2. G. ELSSNER and G. PETZOW, *ISIJ Int.* **30** (1990) 1011.
3. M. G. NICHOLAS and D. A. MORTIMER, *Mater. Sci. Tech.* **1** (1985) 657.
4. Y. IINO, *J. Mater. Sci. Lett.* **10** (1991) 104.
5. Y. IINO, H. USAMI, M. OSHIMODA and T. SAITO, in Proceedings of the First Pacific Rim International Conference on Advanced Materials and Processing (PRICM-1), edited by C. Shi, H. Li and A. Scott (Minerals, Metals and Materials Society, 1992) p. 243.
6. M. L. SHALZ, B. J. DALGLEISH, A. P. TOMSIA and A. M. GLAESER, *J. Mater. Sci.* **28** (1993) 1673.
7. M. L. SHALZ, B. J. DALGLEISH, A. P. TOMSIA and A. M. GLAESER, *Ceram. Trans.* **35** (1993) 301.
8. A. M. GLAESER, M. L. SHALZ, B. J. DALGLEISH and A. P. TOMSIA, *ibid.* **34** (1993) 341.
9. M. L. SHALZ, B. J. DALGLEISH, A. P. TOMSIA, R. M. CANNON and A. M. GLAESER, *J. Mater. Sci.* (in press).
10. F. P. BAILEY and W. E. BORBIDGE, in "Surfaces and Interfaces in Ceramic and Ceramic–Metal Systems", edited by J. A. Pask and A. G. Evans (Plenum, New York, 1981) p. 525.
11. R. V. ALLEN and W. E. BORBIDGE, *J. Mater. Sci.* **18** (1983) 2835.
12. J. KLOMP, in "Science of Ceramics", Vol. 5, edited by C. Brosset and E. Knopp (Swedish Institute for Silicate Research, 1970) p. 501.
13. J. T. KLOMP, *Mater. Res. Soc. Symp. Proc.* **40** (MRS, Pittsburgh, PA, 1985) 381.
14. M. NICHOLAS, R. R. D. FORGAN and D. M. POOLE, *J. Mater. Sci.* **3** (1968) 9.
15. J. E. RITTER and M. S. BURTON, *Trans. AIME* **239** (1967) 21.
16. Yu. V. NAIDICH and V. S. ZHURAVLEV, *Refractories (USSR)* **15** (1974) 55.
17. R. M. CRISPIN and M. NICHOLAS, *J. Mater. Sci.* **11** (1976) 17.

18. M. C. GEE, *Brit. Ceram. Proc.* **34** (1984) 261.
19. C. A. CALOW and I. T. PORTER, *J. Mater. Sci.* **6** (1971) 156.
20. J. A. WASYNCZUK and M. RÜHLE, in "Ceramic Microstructures 86" edited by J. A. Pask and A. G. Evans (Plenum, New York, 1987) p. 341.
21 K. P. TRUMBLE and M. RÜHLE, *Acta Metall. Mater.* **39** (1991) 1915.
22 ASTM Publication E 1019, (ASTM, Philadelphia, PA) pp. 310–11.
23. T. B. MASSALSKI (ed.), "Binary Alloy Phase Diagrams", Vol. 2, (ASM International, Metals Park, Ohio, 1990) pp. 1442–6.
24. J. W. PARK and C. J. ALTSTETTER, *Met. Trans.* **18A** (1987) 43.
25. M. DE GRAEF, B. J. DALGLEISH, M. R. TURNER and A. G. EVANS, *Acta Metall.* **40** (1992) S333.
26. T. C. WILDER, *Trans. AIME Mater.* **236** (1966) 1035.

Received 2 August
and accepted 19 October 1993